A LOW COST TLS BASED LAND MOBILE MAPPING SYSTEM ASSISTED BY PHOTOGRAMMETRY

Um sistema de mapeamento terrestre de baixo custo baseado em um tls assistido por Fotogrametria.

MAJD ALSHAWA
PIERRE GRUSSENMEYER
EDDIE SMIGIEL

Photogrammetry and Geomatics Group, MAP-PAGE UMR 694
INSA de Strasbourg, Graduate School of Science and Technology
24 Boulevard de la Victoire, 67084 STRASBOURG, France
email:majd.alshawa@insa-strasbourg.fr
pierre.grussenmeyer@insa-strasbourg.fr
eddie.smigiel@insa-strasbourg.fr

ABSTRACT

This paper presents an approach of improving navigational data in mobile mapping by using additional photogrammetric measurements. Images taken during a mobile mission are considered as support of GPS/INS while the consumer grade inertial MEMS unit used in the presented mobile system provides only poor estimation of position and attitude even with GPS aid. Nevertheless, this estimation provides initial values for image processing.

Simultaneous bundle adjustment could be done easily with approximate values obtained by GPS/INS solution. The adaptation of our algorithm to meet the case of low cost land mobile mapping is also explained. The feedback to the trajectory determination is discussed from a Kalman decentralized filter point of view. Automatic tie point object coordinates approximation depending on terrestrial laser point clouds is also presented in order to reach a global automatic data processing. The precision of the solution is discussed and assessed by comparing the resulting point clouds with more accurate data sources.

Keywords: TLS, GPS/INS; Navigation; Photogrammetry; Integration; Bundle, Adjustment; Accuracy; Mobile Mapping.

1. INTRODUCTION

Consecutive generations of mobile mapping platforms use more and more sensors. Georeferencing sensors are basically an integration of Global Position System (GPS) and Inertial Measurement Unit (IMU). IMUs of a high grade are often used on board of these systems. The measurements of such units drift slightly with time and could be trustful for some tens of seconds without external aid. The GLONASS satellites have been integrated with GPS ones to ensure a better constellation and a better availability of calculated positions consequently. Odometers and digital barometers are used also to bridge GPS outages and lack of precision in altitude respectively. Many algorithms are used to integrate all these sensors and to compensate the weak points of either.

Low cost systems could have a consumer grade IMU and one GPS antenna which is the minimal configuration to provide an acceptable navigation solution. The designers of these systems try to compensate the imprecision of this configuration by adding other low cost sensors and using more adapted computation methods. This article belongs to this category of design. Photogrammetry is chosen as a support to navigation because of its consistency with the low cost aspect. A single camera is used by the laser based mobile system to support the navigation part rather than an imaging sensor. This article shows how a camera could be used as position and attitude sensor.

After a brief scan of the related literature, the necessary operations to implement the photo information as corrections to the six degree of freedom (6DoF) of navigation are explained. Calibration and synchronisation issues are approached. The adaptation of bundle adjustment algorithm is explained. The decentralized Kalman filter used to integrate GPS/INS and INS/photo in parallel is shown afterwards. Some experimental results and interesting notes are finally discussed.

Photographic and video cameras are often used by mobile mapping systems as imaging sensors. The classic photogrammetric products or the texturing of laser point clouds are typical outputs of these cameras. Nevertheless some systems use cameras differently. DA SILVA et al (2003) do not use any IMU in their system. The continuity of the stereo video images insures the attitude calculation whatever the condition of GPS mask. The videos are processed with SLAM (Simultaneous Localization And Mapping) logic rather than the photogrammetric one. GAJDAMOWICZ et al (2007) use bundle adjustment to obtain the position and the attitude of the camera and consequently to recalculate the GPS/INS 6DoF. This procedure is used finally to refine the precision of final point cloud acquired simultaneously. SHI et al (2008) use two sets of stereo camera to collect images. The images are used to texture the laser data and to improve the navigation data. The present paper goes beyond the information given by these articles. A method of finding the approximated object coordinates for tie points is explained. The decentralized Kalman filter approach is introduced to respect the requirements of

systems that use a stable coupled GPS/INS for which not all the information and the method are available (principle of black box).

2. DESIGNED SYSTEM

The designed prototype consists of a RTK GPS and an AHRS MEMS coupled to a High Sensibility GPS (HSGPS). A TLS (Terrestrial Laser Scanner) was used as the principal mapping sensor in the system. More detailed information could be found in (ALSHAWA et al. 2008). The poor position is due principally to the interruption of RTK GPS and to the incapacity of the HSGPS to regain the interruption precisely. On the other hand, the precision of the attitude is generally low (1-2 degrees) because of the limitations of MEMS magnetometers, accelerometers and gyroscopes.

For the purpose of navigation enhancement, a Canon EOS 5D digital camera is used. It enables to capture up to one photo per second by means of a computer remotely command program. The movement of the platform mobile has almost no effect on the quality of the obtained photos. Wide angle lens line-up is used to guaranty high overlay between photos.

The accuracy of the built-in clock of the camera is of one millisecond. This accuracy is sufficient for the low speed of our system (1msec gives an error of 1mm at a velocity of 1 m/sec). Indeed, fractions of seconds are not provided by default in photos header. The SDK (Software Developper Kit) is used to contain the millisecond timestamp in the EXIF file of each photo. The synchronization between the computer clock and the camera built-in clock has to be always maintained by the program of camera remote command. The knowledge of the precise photo timestamp enables the determination of GPS/AHRS measurements for each camera station. We have also to know the spatial relations between the GPS, the AHRS, and the camera to be able to compare the photogrammetric computation results with navigation measurements. These spatial relations are called “boresight calibration”

3. BORESIGHT CALIBRATION

Assuming a rigid installation of all system components, the boresight calibration means the determination of two constants: the distance a^b between the phase center of the GPS and the center of camera sensor and the rotation matrix R_b^c between the body coordinates frame (AHRS frame) and the camera frame. The platform is fixed in good GPS reception conditions and the AHRS is configured in a no dynamic motion mode. When the AHRS is stabilized at a correct alignment, we can start logging GPS and AHRS data for some minutes. In the same time, a calibration entity with known object point coordinates is photographed. The spatial resection of the photo could be done with the aid of approximations explained in figure 1.

The eccentricity a^b is measured by tacheometric methods and refined by calculation.

$$a^b = R_g^c\left(r_{GPS}^g - r_c^g\right) \quad (1)$$

$$R_c^b = R_c^g . R_b^{g^{-1}} \quad (2)$$

where: R_g^c : the rotation matrix from object (geodetic) frame to camera one (output of photo resection)

r_c^g: the position of the center of the camera sensor in the geodetic frame (output of resection computation too)

r_{GPS}^g : the geodetic position for the GPS antenna

R_b^g : the rotation matrix from body (vehicle) frame to the geodetic one (results from AHRS averaged measurement during all calibration time).

Figure1 - Approximations for the six elements of exterior orientation for the calibration phase:
$X_{L0} = X_{GPS}$, $Y_{L0} = Y_{GPS}$, $Z_{L0} = Z_{GPS}$ (the object-coordinates of the principal point)
ω_0 = roll + $\pi/2$, ϕ_0 = -yaw, κ_0=pitch (the orientation of the camera).

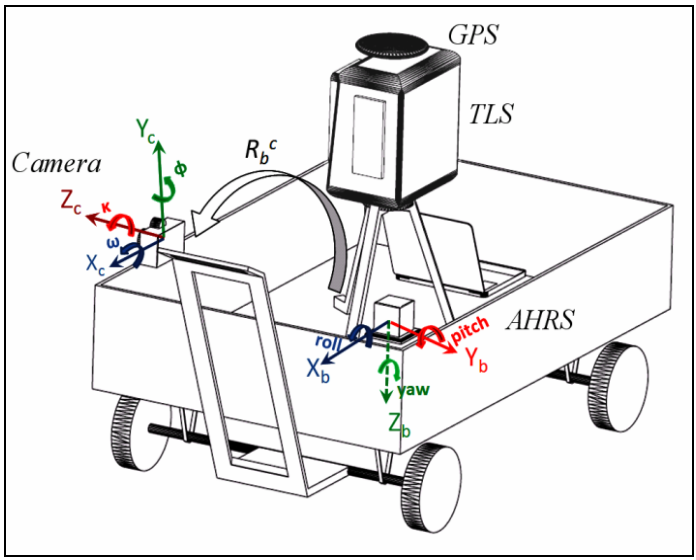

4. APPROXIMATE TIE POINTS COORDINATES

In order to accomplish bundle adjustment step, tie points have to be detected between the photos. Automatic homogenous point matching is not discussed in this paper. Nevertheless, finding object coordinates approximation for these points is the subject of this paragraph.

The direct georeferencing of photos does not produce point coordinates directly (unlike laser case) because of the variable scale factor *s* in the equation:

$$r_p^g(t) = r_{GPS}^g(t) + R_b^g(t)\left[a^b + s_p R_c^g r_p^c(t)\right] \quad (3)$$

where:

r_p^g : coordinates of a point p in the geodetic frame

r_p^c : coordinates of the point *p* in the camera frame

t: instant of photo shooting

The determination of approximations consists of three steps:

1. Creation of equation of the light ray that passes through the chosen point and the principal point: This straight line could be expressed in the camera 3D frame by its origin point (0,0,0) and the direction vector $v = \left(x_p y_p - f\right)^T$ where $x_p y_p$ are the point coordinates in camera sensor system (corrected from radial and tangential distortion)

2. Line equation transformation into the geodetic frame: The transformation is achieved by applying a shift T_l to origin point and a rotation R_l to the direction vector. T_l and R_l are given by the following relations:

$$T_l = r_{GPS}^g(t) + R_b^g(t).a^b \quad (4)$$

$$R_l = R_b^g(t).R_c^g \quad (5)$$

Line known point is so equal to T_l while the direction vector is equal to $R_l.v$

3. Searching among the georeferenced laser point cloud the nearest one to the mentioned line: In order to simplify this operation, one can use the equation 3 with an averaged scale factor $s_{p\text{-}av}=H/F$ (H is the mean distance between the camera and the scanned object. A voxel of variable dimension (according to object complexity and scan density) is adopted as the convex hull containing the researched point. The distances of all points in this voxel to the calculated light ray are calculated by the relation:

$$d_j = \frac{norm\left[\left(R_l.\left(x_p y_p - f\right)^T\right) \otimes \left(T_l - r_j\right)\right]}{norm\left(R_l.\left(x_p y_p - f\right)^T\right)} \quad (6)$$

The laser point with the minimal distance is chosen as approximated coordinates. If the light ray intersects with the point cloud in more than one point, the nearest to camera station is chosen.

Figure 2 - Computation of approximate object coordinates for a point *p* measured on a photo.

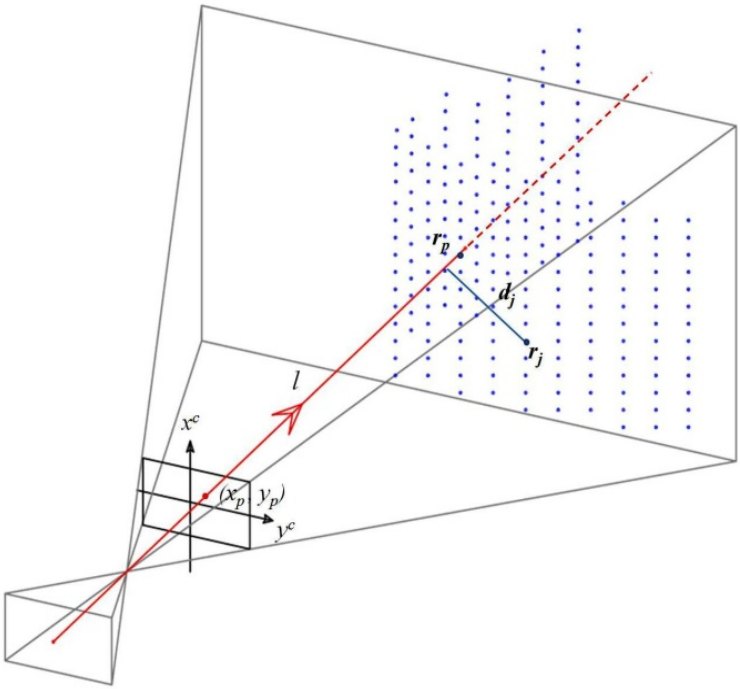

5. SIMULTANEOUS BUNDLE ADJUSTMENT

The available inputs to the bundle adjustment algorithm are the observed photo point coordinates and the observed six elements of exterior orientation which are the unknowns too. On the other hand the approximate object coordinates, even not a sought unknown, have to be updated during the iterations of bundle adjustment algorithm. We do not involve the equations of GPS or INS in the algorithm as in (EBADI and CHAPMAN, 1995) because of the lack of the ground control points.

Two sort of equation are used; the classic colinearity equations for each point *j* in each photo *i*:

$$F_x = x_j - x_0 + f\frac{r_{11}(X_j - X_L) + r_{12}(Y_j - Y_L) + r_{13}(Z_j - Z_L)}{r_{33}(X_j - X_L) + r_{32}(Y_j - Y_L) + r_{33}(Z_j - Z_L)} \tag{7}$$

$$F_y = y_j - y_0 + f\frac{r_{21}(X_j - X_L) + r_{22}(Y_j - Y_L) + r_{23}(Z_j - Z_L)}{r_{31}(X_j - X_L) + r_{32}(Y_j - Y_L) + r_{33}(Z_j - Z_L)} \tag{8}$$

where x_i, y_i: photo coordinates for the measured point
X_i, Y_i, Z_i: object approximated coordinates
r_{11}, r_{12} ….. r_{33}: the components of the rotation matrix $R^g_{c\ (\omega,\varphi,\kappa)}$ for the i^{th} photo

The second kind of equations is the difference between the observed and the unknown photo exterior orientation elements ($X_L, Y_L, Z_L, \omega, \varphi, \kappa$):

$$\begin{aligned} G_{X_L} &= X_L^{observed} - X_L \\ G_{Y_L} &= Y_L^{observed} - Y_L \\ G_{Z_L} &= Z_L^{observed} - Z_L \\ G_{\omega} &= \omega^{observed} - \omega \\ G_{\phi} &= \phi^{observed} - \phi \\ G_{k} &= k^{observed} - k \end{aligned} \tag{9}$$

For a point *j* measured in the *i*th photo, the linearised observation equation is written as follows:

$$\begin{pmatrix} J_{eo} & J_{coor} \\ -I_{6\times6} & 0_{6\times3} \end{pmatrix} \cdot \begin{pmatrix} \Delta_{eo} \\ \Delta_{coor} \end{pmatrix} = \begin{pmatrix} F \\ G \end{pmatrix} \tag{10}$$

with the Jacobians:

$$J_{eo} = \begin{pmatrix} \frac{\partial F_x}{\partial p} & \frac{\partial F_y}{\partial p} \end{pmatrix} \qquad p \in \{X_L, Y_L, Z_L, \omega, \varphi, \kappa\} \tag{11}$$

$$J_{coor} = \begin{pmatrix} \frac{\partial F_x}{\partial p} & \frac{\partial F_y}{\partial p} \end{pmatrix} \qquad p \in \{X_j, Y_j, Z_j\} \tag{12}$$

the misclosure vectors:

$$F = (-F_x \quad -F_y) \tag{13}$$

$$G = (G_{X_L} \quad G_{Y_L} \quad G_{Z_L} \quad G_{\omega} \quad G_{\varphi} \quad G_{\kappa}) \tag{14}$$

and the corrections to be added to the initial values

$$\Delta_{eo} = (\delta X_L \quad \delta Y_L \quad \delta Z_L \quad \delta\omega \quad \delta\varphi \quad \delta\kappa)^T \tag{15}$$

$$\Delta_{coor} = \left(\delta X_j \quad \delta Y_j \quad \delta Z_j\right) \tag{16}$$

The formation of normalized equations and the solution details could be found in (WOLF and DEWITT, 2000). The corresponding weight for the measurement of exterior orientation elements could be derived from GPS/AHRS integration Kalman solution. The position and orientation solution of the camera in the geodetic frame have to be transformed into AHRS one using the calibration constants. In this stage, we have two sets of navigation measurement for some instants; those of photo shooting. The next step is to integrate and generalize the photo solution.

6. GPS/AHRS/PHOTO INTEGRATION

GPS/AHRS integration achieved by the embedded processor of the AHRS unit is provided by a Kalman filter with loosely coupled architecture. GPS corrections to the AHRS full navigation solution are the position and the velocity. These corrections are supplied in real time at 4 Hz frequency when the GPS locks on a valid solution. Otherwise the AHRS may have no GPS support for few seconds during GPS masks. The implementation of the embedded Kalman filter is not known, but it is possible to reconstitute the precisions of results at every moment of measurement.

On the other hand, the bundle adjustment is able to produce corrections of position and attitude at a frequency totally mastered by user and without interruption.

The depicted case evokes the use of decentralized Kalman filter described in (BROWN AND HWANG 1997). Two local filters will be combined; the first one is the interior GPS/AHRS and the second one is the photo/AHRS which is the subject of the next paragraph.

The effect of the distances between the centers GPS-IMU and Camera-IMU (known as the problem of lever arm) is corrected as proposed in (SHIN, 2001).

6.1 Photo/AHRS

Magnetometers participation is omitted in this stage of solution since their accuracy is not sufficient for the refinement. The filter becomes consequently photo/INS integration. State vector and perturbation equations are considered as proposed in (SHIN, 2001). The state vector consists of the position, the velocities and the attitude. The state noise consists of gyros and accelerometer biases. Prediction loop remains the same while the update one changes. At each instant $k=k_i$ when a photo is taken, the update is done with the following correction model:

$$z_{2k} \approx H_{2k} \,.\, x_{2k} + w_{2k} \tag{17}$$

where the index "2" distinguishes the second local filter. z_{2k} is the correction vector:

$$Z_{2k} = \begin{pmatrix} lat_{INS} - lat_{photo} \\ long_{INS} - long_{photo} \\ h_{INS} - h_{photo} \\ roll_{INS} - roll_{photo} \\ pitch_{INS} - pitch_{photo} \\ yaw_{INS} - yaw_{photo} \end{pmatrix} \tag{18}$$

the measurement matrix $H_{2k} = \partial Z_k / \partial p$: $p \in x_{2k}$ (state vector) is equal to:

$$H_{2k} = \begin{pmatrix} I_{3\times3} & 0_{3\times3} & 0_{3\times3} \\ 0_{3\times3} & 0_{3\times3} & I_{3\times3} \end{pmatrix} \tag{19}$$

The measurement noise w_{2k} is not used in the computation but its covariance matrix R_{2K} which is taken equal to the covariance matrix resulted from bundle adjustment solution for the concerned photo.

6.2 Decentralized Kalman filter

Since both of local filters share the same state, they run at the same frequency. At end of each computation of individual states and covariance matrix, the fusion is achieved using the following relations (WEI and SCHWARZ, 1990):

$$\hat{x}_{k\,d}^{+\,-1} = P_{k\,d}^{+} \left[P_{k\,d}^{-\,-1} \hat{x}_{k\,d}^{-} + (P_{1k}^{+\,-1} \hat{x}_{1k}^{+} + P_{2k}^{+\,-1} \hat{x}_{2k}^{+}) - (P_{1k}^{-\,-1} \hat{x}_{1k}^{-} + P_{2k}^{-\,-1} \hat{x}_{2k}^{-}) \right] \tag{20}$$

$$\hat{P}_{k\,d}^{+\,-1} = P_{k\,d}^{-\,-1} + (P_{1k}^{+\,-1} - P_{1k}^{-\,-1}) + (P_{2k}^{+\,-1} - P_{2k}^{-\,-1}) \tag{21}$$

where $\hat{x}$ is the mean estimation for the state vector and $\hat{P}$ is the mean estimation of the covariance matrix.

The indicator d symbolizes the decentralized result, k the instant of measurement, super minus for the "a priori" estimate and super plus for the "a posteriori" estimation. The "1" sub-index refers to the GPS/AHRS local filter results while the "2" refers to the Photo/INS local filter.

Corrections are fed forward for first local filter (GPS/AHRS) because of the non-accessibility to its equations. On the other hand, the corrections of photo/INS

could be fed back but we chose to feed them forward for reason of consistency with the first filter.

7. EMPIRICAL STUDY

The presented example is one of the paths run by the prototype mobile. The velocity is about 2 Km/h and the rate of photo shooting is every 5 sec. The overlap ratio between the photos is about 60% which guaranties the bundle adjustment process. Figure 3 shows a panorama made of some taken photos.

Figure 3 - Panorama of some photos taken during the mobile missions (lens focal length equal to 28 mm)

The studied sample consists of 12 photos covering about 40m of urban façades. The average distance between the mobile platform and the façades is about 15m.

7.1 Trajectometry processing

The RTK GPS (Leica® TP1200) could only measure few points not well distributed. In contrast, the HSGPS (Ublox® EVK-5T) did not miss any point. Figure 4 illustrates the full coverage low accuracy HSGPS and the accurate GPS measurements. The camera stations are also placed by mean of the corresponding timestamps.

Figure 4 - HSGPS measurements (blue), the RTK GPS measurements (green) and the camera positions (red).

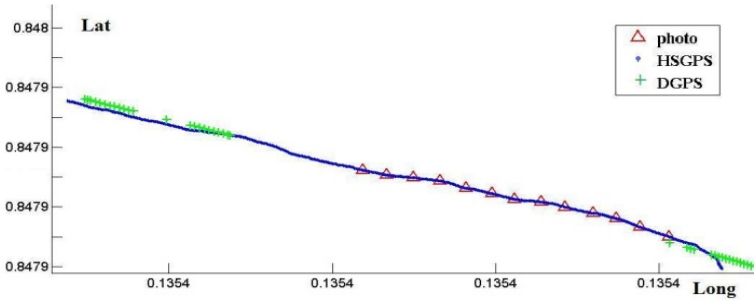

The two kinds of GPS observations are merged using two step method; the HSGPS measurements are shifted towards the RTK ones and then a weighted curve fitting is applied. This method is described in (ALSHAWA et al. 2008).

7.2 Laser point cloud computation

Laser point cloud is calculated without taking into account the participation of photos in the solution. The horizontal resolution of the acquired point cloud is about 15 cm and the general precision of the point cloud is about 15-20 cm. This precision is calculated with error propagation method as explained in (ALSHAWA et al. 2007). The precision of approximated coordinates for the tie points is therefore about 20 cm. The final shape of the estimated path travelled by the mobile prototype and the point cloud are shown in figure 5.

Figure 5 - First computation of laser point cloud and the positions of camera stations (in red).

7.3 Bundle adjustment computation

The triangulation of the 12 photos computation is achieved with 138 degrees of freedom. The difference between the calculated values of exterior orientation elements and the input ones are depicted in table 1 and figure 6.

Table 1 - Differences between input and output values from bundle adjustment algorithm

Photo	Δx_{cm}	Δy_{cm}	Δz_{cm}	$\Delta roll_{deg}$	$\Delta pitch_{deg}$	Δyaw_{deg}
1	-1,1	0,3	-0,8	0,05	0,06	1,26
2	-2,4	1	-1,8	0,10	0,11	0,72
3	-1,1	0,3	-2,4	0,12	0,01	0,81
4	-1	0,3	-2	0,11	0,0	0,34
5	-1,8	0,6	-2,7	0,13	0,01	0,04
6	0,1	-0,5	-2,9	0,12	-0,09	-0,20
7	0,9	-1,2	-2,4	0,11	-0,14	-0,59
8	1,7	-1,3	-2,1	0,09	-0,14	-0,74
9	1,5	-1,3	-2,0	0,09	-0,16	-0,66
10	1,5	-0,6	-2,0	0,08	-0,11	-1,15
11	2,4	-1,5	-1,9	0,10	-0,19	-1,34
12	1,9	-1,5	-1,1	0,07	-0,18	-1,05

The non-systematic distribution of the residuals emphasizes the lack of synchronization or calibration blunders. On the other hand, the degradation of heading residuals from positive to negative indicates the existence of a drift not totally corrected by the HSGPS/AHRS filter. Heading residuals are obviously greater than the roll or the pitch ones which is a classic problem of inertial navigation (the vertical gyroscope is less accurate than the horizontal one). The yaw angle will be thus our case study for the next analyses.

Table 2 depicts the precision of the bundle adjustment computation which is deduced directly from the covariance matrix. The calibration errors are not taken into account in this table.

Table 2 - Root mean square errors of exterior orientation elements.

photo	$\sigma_{x\ mm}$	$\sigma_{y\ mm}$	$\sigma_{z\ mm}$	σ_{roll} $_{deg\times10^{-4}}$	σ_{pitch} $_{deg\times10^{-4}}$	σ_{yaw} $_{deg\times10^{-4}}$
1-12	4,5	4,5	4,2	9,6	9,7	9,1

The values exposed above are too similar for all photos. This could be interpreted by the input weight matrixes. All tie points have exactly the same precision and the GPS/AHRS provided input observations have almost the same precision too. The magnetic and inertial mechanization have been done in continuous HSGPS aiding which explains the close precision values.
The residual output from the bundle adjustment step (Table.1) will be the input for the INS/photo local filter exposed below.

7.4 Photo/INS integration

The local filter of photo/INS integration runs at the same output rate of GPS/AHRS one (20 Hz) and not at the frequency of laser scanning (~2000 Hz). The migration between the two rates is achieved by linear interpolation.

Since the precision of photogrammetric solution is remarkably higher than the navigation one, it dominates the solution. Figures 6 shows the relative situation for the yaw angle measured by the AHRS/GPS and deducted from triangulation solution. Figure 7 illustrates the crucial modifications of yaw curve after applying the Photo/INS local extended Kalman filter.

Figure 6 - Comparison between the yaw measured by AHRS/GPS (blue) and calculated by the bundle adjustment (red)

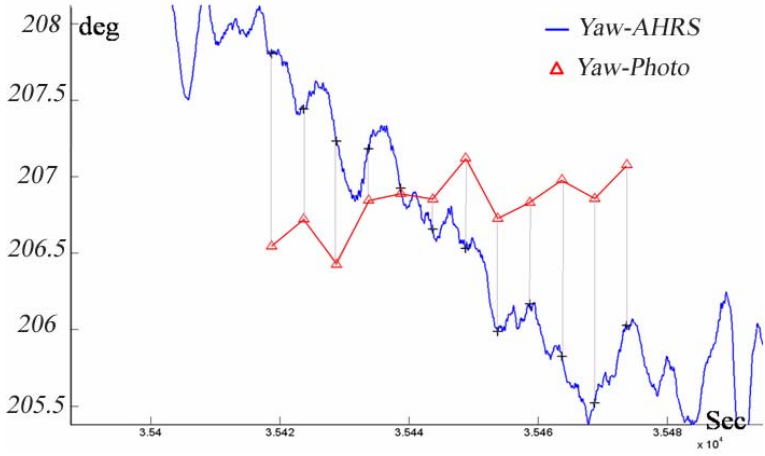

Figure 7 - Yaw angle resulted from Photo/INS extended Kalman filter

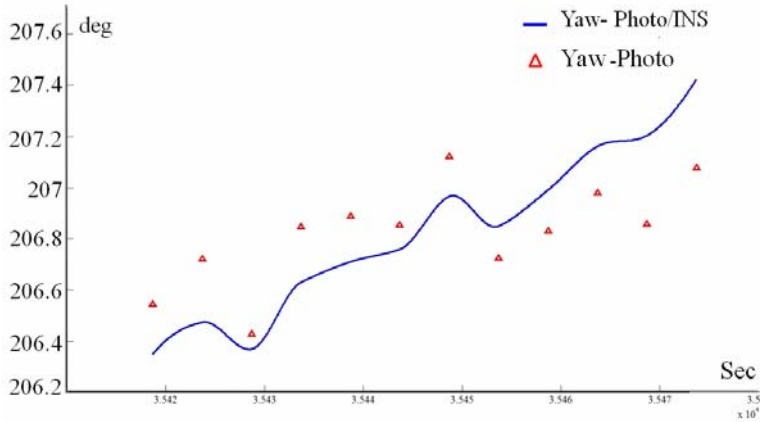

7.5 Integration (INS/photo + GPS/AHRS)

In the last paragraph, the integration between the inertial raw data and the result of bundle adjustment is exposed. This filter is achieved in post-processing. On the other hand the raw inertial and magnetic data undergo other integration; with the GPS and in real time. Both local filter results are combined by means of equation (20,21). The final shape for our case study is illustrated in the figure 8.

Figure 8 - The result of decentralized Kalman filter (red curve).

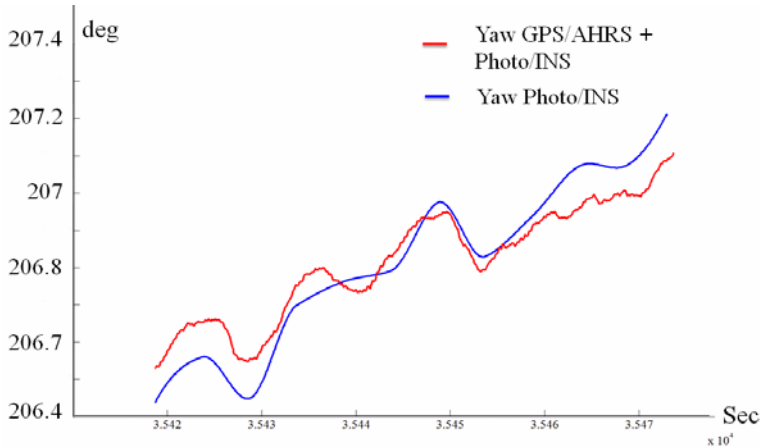

One can note that the integration of GPS corrections has slightly modified the general inclination of the curve of Photo/INS yaw. While the frequency of the GPS corrections is greater than the photo one, the curve becomes less smooth.

In order to quantify the precision of the last estimation, the mean square errors for weight unit corresponding to the previous estimation P_k^{yaw} is plotted in figure 9.

$$P_k^{yaw} = \frac{\sqrt{P_{k(9,9)}}}{norm(diag(P_k))} \tag{20}$$

where P_k is the covariance matrix of decentralized filter calculated at the instant k.

Figure 9 - Mean square error corresponding to the final computation of the yaw angle.

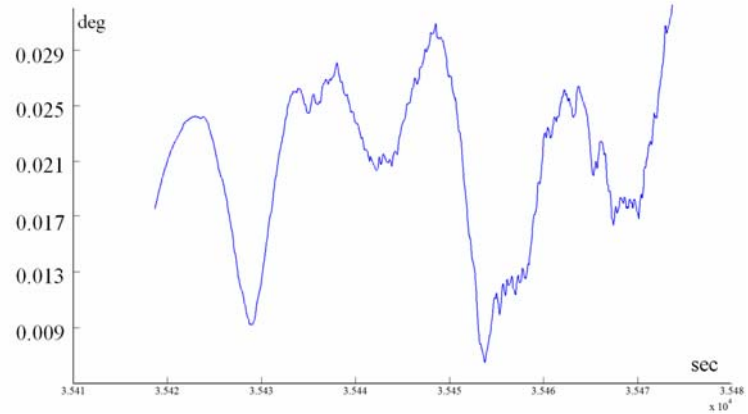

Though one expects to find a number of "precision picks" equal to the number of photos, the number seems to be less. Some photos do "succeed" to enhance the yaw inertial measurement more than others. The precision of yaw is highly correlated with the other states of Kalman filter (3 positions, 3 velocities and 2 angles) which affect the precision differently.

The best recorded precision is closely related to the the photogrammetric solution (0.09 deg). It rises up to 0.03 deg for the farthest (chronologically) points from camera stations.

7.6 Final point cloud computation

The final point cloud is calculated by direct geo-referencing using the position and the attitude output from the last step. The changes between point clouds calculated with and without the photogrammetric contribution could be found by calculating the distance between points. Both of calculated point clouds share the time indexing. The distance between the two calculated positions for the same laser measurement taken in the same instant is calculated and mapped on the photo-corrected cloud (figure 10). The stated change is mainly due to yaw, X and Y corrections.

Figure 10 - Re-calculated point cloud taking into account the photogrammetric corrections.

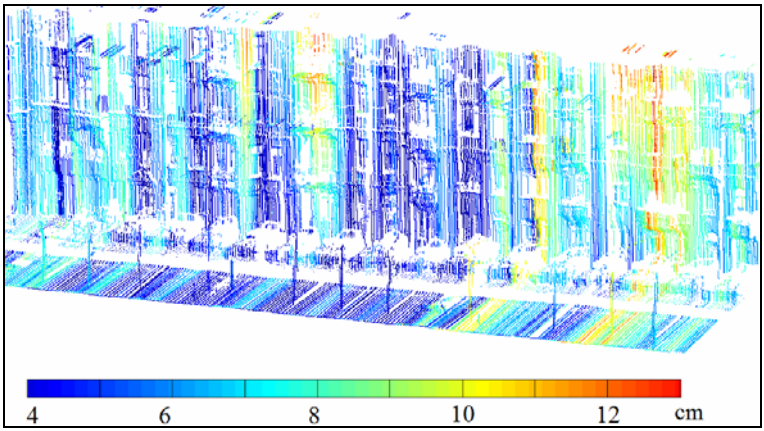

Though the visual enhancement (as noticed in figure 11), further tests are needed to verify the result. In fact, the comparison with an external data source could emphasize or reject the accuracy improvement which is the subject of the next paragraph.

Figure 11 - Improvement occurred to the mobile point cloud after applying the photogrammetric contribution (GPS/AHRS/photo point cloud at the right side).

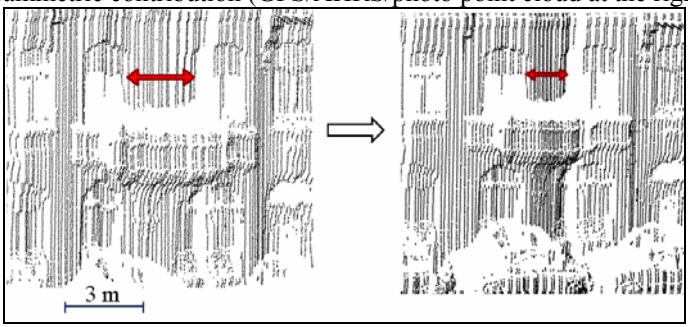

7.7 Accuracy assessment

The result of the suggested method has been compared with a more accurate data source (reference: a point cloud generated from the geo-referenced photos). The result of the bundle adjustment (elements of exterior orientation and the most accurate tie points resolved in object space) are uploaded to PhotoModeler Scanner® software. A dense point cloud was created with a precision estimated

generally of few centimeters. The calculated laser point cloud overlapped with the photogrammetric one is shown in figure 12.

Figure 12 - Superposition between the laser (blue) and the photo (red) point clouds.

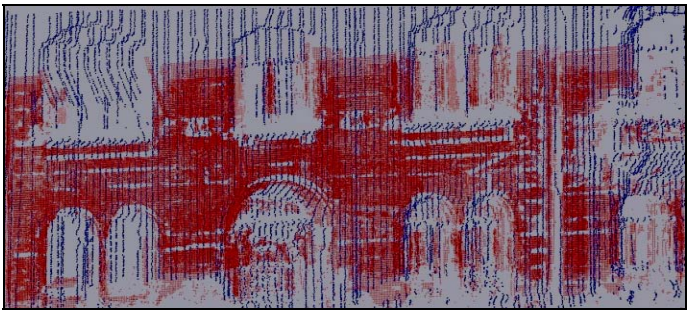

While trying to use ICP method to refine the consolidation between the two point clouds, an error (based on rotation and shift) of 10 cm is stated. This error could be considered as an indicator of the difference between the point clouds. The same indicator is equal to 15 cm for the point cloud calculated without photogrammetric aid (shown in figure 5).

For a better comprehension of error distribution, the distance between both point clouds was mapped using CloudCompare[1] software. Figure 13 illustrates the error mapping colors projected on mobile laser point cloud. Distances less than 20 cm are only mapped in order to have better color scale representation.

Figure 13.a - Part of mobile laser point cloud coloured with respect of the photo-generated one.

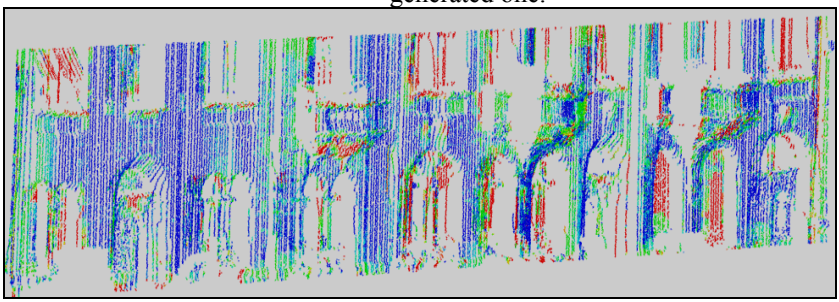

[1] Propriety of EDF and TELECOM ParisTech.URL: http://rd.edf.com/edf-fr-accueil/edf-recherche--developpement/logiciels-et-codes/cloudcompare-601069.html

The histogram of the occurrence of each distance is showed in the figure 13b. One can note that 78% of points have accuracy better than 10 cm. The percentage of the points having accuracy less than 15 cm is about 10%. These points are found mainly in recessed parts (doors, gates and windows). In areas as windowpanes or opened doors, the difference is due to the difference in incidence angle between laser and light rays (photogrammetric reconstruction and laser scanning). Indeed, the precision of a point cloud generated by photogrammetric methods depends on many factors. For instance, self occlusion areas do not provide the best reference for such comparison.

Figure 13.b - Histogram illustrating the distribution of the distances between photogrammetric and laser point clouds.

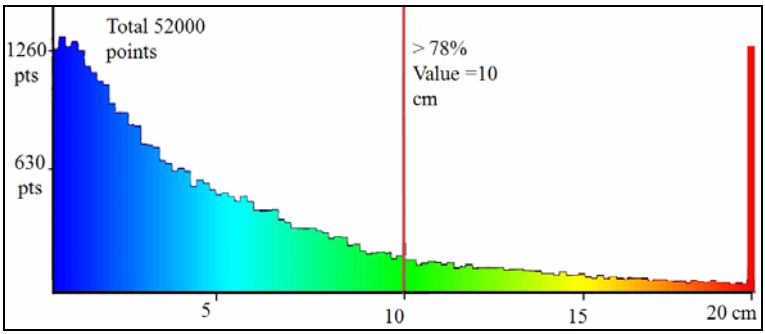

8. CONCLUSION AND FUTURE WORKS

The contribution of photogrammetric corrections to the navigation solution has been depicted in this article. Although the use of a camera as a navigation sensor did not yet achieve its maturity, its contribution to navigation improvement was proven. Photo orientation by bundle adjustment could be a more important solution than the GPS one especially in urban areas. Nevertheless, it is impossible to be applied in real time. In order to achieve a better accuracy, the frequency of photo shooting have to be increased which imposes more photogrammetric processing.

The future work will be dedicated to the automation and the ergonomic aspect of the method (especially in the tie point detection step). With a high automation degree, more photos could be taken in order to constraint the accelerometers and the gyro drift. This could also avoid the interruption of the bundle because of optical obstacles.

The proposed method gets tie points object coordinates approximations from the primary computation of laser point cloud. The laser point cloud is corrected after applying the photogrammetric measurements. This could help to recalculate a

new object position of tie points. Consequently, it would be possible to apply the suggested method in an iterative manner.

REFERENCES

ALSHAWA M.; GRUSSENMEYER P.; SMIGIEL E, LANDES, T. 2007. Integration of a Terrestrial Lidar on a Mobile Mapping Platform: first experiences. 5th International Symposium on Mobile Mapping Technology MMT'07, 29-31 may, 2007, Padua, Italy. 6 pages.

ALSHAWA M.; GRUSSENMEYER P.; SMIGIEL E. Integration of a TLS in a low cost mobile mapping system. VSMM 2008 - Conference on Virtual Systems and MultiMedia Dedicated to Digital Heritage. Limassol, Cyprus, October 20th - 25th, p.1-8, 2008.

BROWN S.A.; HWANG P.Y. C., Introduction to random signals and applied Kalman filtering with matlab. exercises and solutions, 3rd edition. ISBN: 978-0-471-12839-7. 496 pages, 1997.

DA SILVA, J. F. C.; DE OLIVEIRA, C.P.; Gallis, B. A.R. Development of a low cost mobile mapping system: a South American experience. *Photogrammetric record*, v. 18, n. 101, p.5-26, 2003.

EBADI, H.; M.A. CHAPMAN, An experience on gps assisted aerotriangulation. Proceedings of the 7th international conference on Geomatics, June 13-15, Ottawa. 1995.

GAJDAMOWICZ, K.; ÖHMAN, D.; HOREMUZ, M. Mapping and 3D modelling of urban environment based on Lidar,GPS/IMU and image data. Proceeding of 5th International Symposium on Mobile Mapping Technology (MMT2007) Padova, Italy. 29-31 may 2007.

SHI, Y.; SHIBASAKI R.; SHI, Z.C. Towards automatic road mapping by fusing vehicle-borne multi-sensor data. The International Archives of the Photogrammetry, Remote Sensing and Spatial Information Sciences. v. XXXVII. Part B5. Beijing 2008.

SHIN, E.H., Accuracy improvement of low cost ins/gps for land applications. University of Calgary. UCGE reports number 20156. 119 pages, 2001.

WEI, M. and SCHWARZ, K.P. Position Location and Navigation Symposium, Record. The 1990's - A Decade of excellence in the navigation sciences. IEEE PLANS '90. p. 429-435, 1990.

Wolf, P. R.; DEWITT B. A. Elements of photogrammetry: with applications in GIS (3rd edition). ISBN-10: 0072924543 ISBN-13: 9780072924541. 608 pages, 2000.